**Structure, Volume *23***

## Supplemental Information

# Molecular Basis of MgATP Selectivity of the Mitochondrial SCaMC Carrier

**Changqing Run, Qin Yang, Zhijun Liu, Bo OuYang, and James J. Chou**

# Supplemental Information

## Molecular Basis of MgATP Selectivity of the Mitochondrial SCaMC Carrier

Changqing Run[1, 2], Qin Yang[3], Zhijun Liu[1], Bo OuYang[1, 2]*, James J. Chou[1, 2, 3]*

### Supplemental Figures

**Figure S1** Sequence Alignment between AAC and $SCaMC_{TMD}$ for showing the conserved residues between the two nucleotide transporters. *Relates to Figure 1, to show the similarity between AAC and SCaMC.*

**Figure S2** Comparison of the effects of MgATP, ATP and $Mg^{2+}$ on $SCaMC_{TMD}$ chemical shifts. *Relates to Figure 2 to show that MgATP and ATP are substrates of SCaMC whereas $Mg^{2+}$ is not.*

**Figure S3** Estimation of MgATP binding affinity using chemical shift titration data. *Relates to Figure 2 & 3, to show that the binding affinity calculated from chemical shift changes and MnATP/MgATP broadening/recovery are consistent.*

**Figure S4** The $Mn^{2+}$/$Mg^{2+}$ titration showing the inability of $Mg^{2+}$ cation alone to displace the paramagnetic $Mn^{2+}$. *Relates to Figure 3, to show that MgATP induced specific displacement of MnATP is not due to non-specific binding of $Mg^{2+}$ cations.*

**Figure S5** The nucleotide transport activity of $SCaMC_{TMD}$ showing a much higher selectivity for MgATP over ATP. *Relates to Figure 4, to show that the liposome assay functioned as expected.*

**Figure S6** Comparison of the NMR spectra of the WT and mutant $SCaMC_{TMD}$ showing negligible effect of the mutations on the transporter structure. *Relates to Figure 4, to show that the point mutations have essentially no effect on the protein conformation.*

**Figure S7** The inability of $SCaMC_{TMD}$ to bind MgATP by mutation of D361A. *Relates to Figure 3 & 4, to show that D361 is the key residue for MgATP binding.*

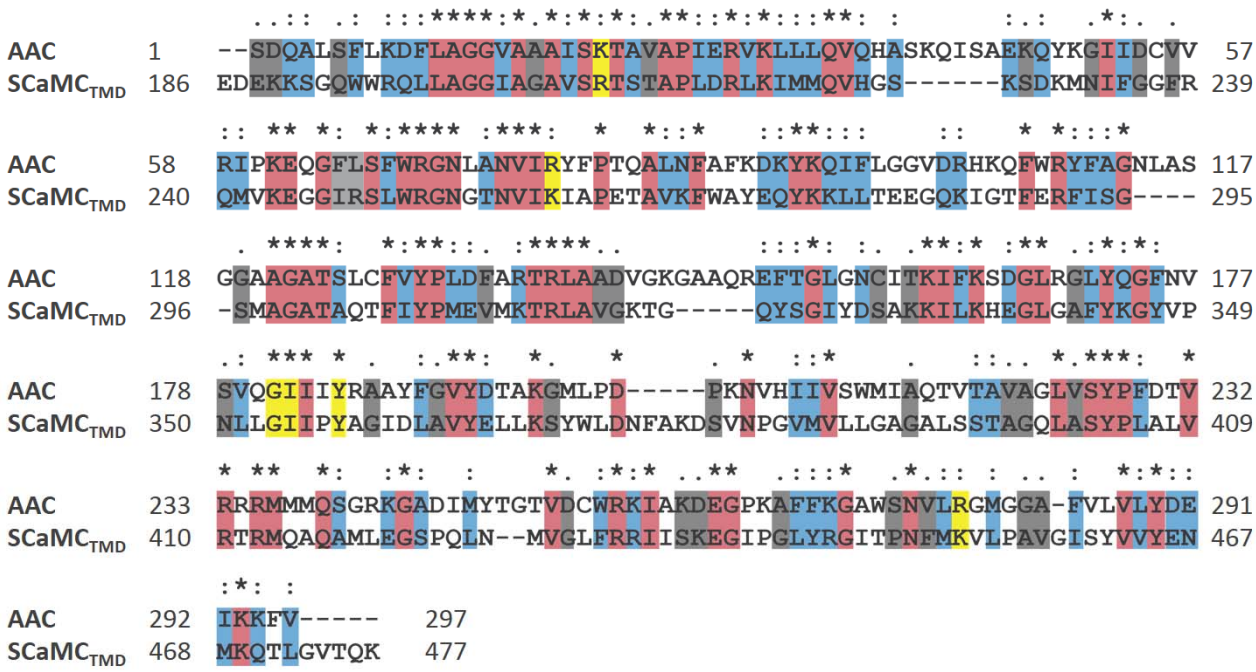


**Figure S1.** Sequence alignment between AAC and SCaMC$_{TMD}$ for showing the conserved residues between the two nucleotide transporters. Residues strictly conserved in both AAC and SCaMC$_{TMD}$ are indicated by asterisks '*' and shaded in red; partially conserved are indicated by colons ':' and shaded in blue; much less conserved are indicated by dots '.' and shaded in gray. The six residues involved in ATP binding are highlighted in yellow.

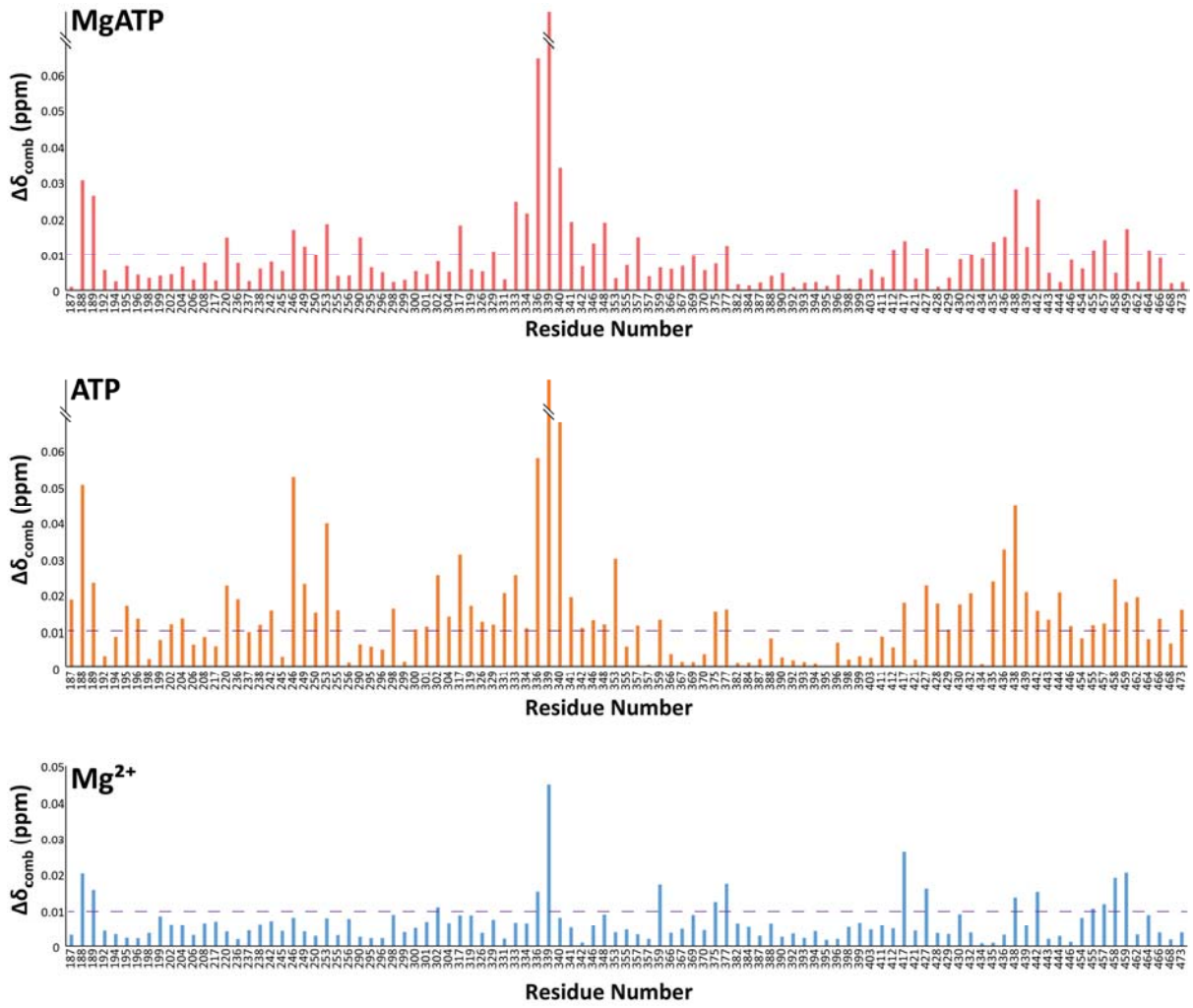


**Figure S2.** Comparison of the effects of MgATP, ATP and $Mg^{2+}$ on $SCaMC_{TMD}$ chemical shifts. Spectra were recorded using a 0.2 mM $^{15}N$ labeled sample without substrates and with the addition of 16.7 mM MgATP (upper panel), 16.7 mM ATP (middle panel) or 16.7 mM $Mg^{2+}$ (lower panel). Only resolved peaks are depicted here. The dashed lines correspond to 0.01 ppm.

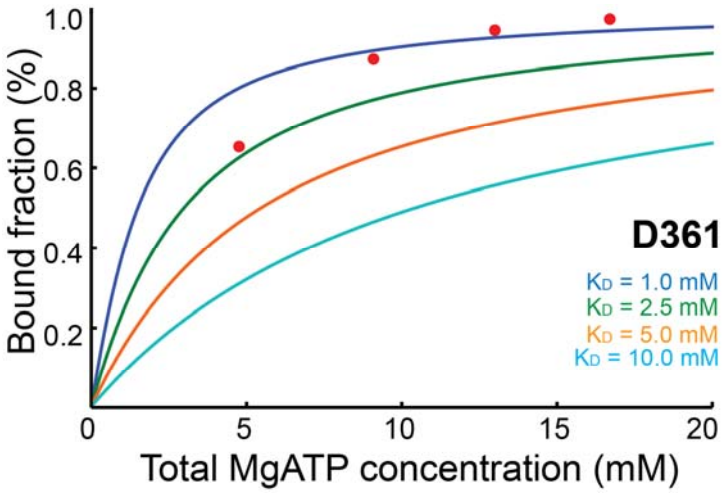


**Figure S3.** Estimation of MgATP binding affinity using chemical shift titration data. Binding affinity simulation curves for 0.4 mM $SCaMC_{TMD}$ titrated with substrates with affinities of 1.0 mM, 2.5 mM, 5.0 mM and 10 mM are colored in blue, green, orange and cyan, respectively. Following equation was used for calculating the MgATP bound fraction of $SCaMC_{TMD}$ $\frac{[PS]}{[P_{total}]} = \frac{([P_{total}]+[S_{total}]+Kd) \pm \sqrt{([P_{total}]+[S_{total}]+Kd)^2 - 4[P_{total}][S_{total}]}}{2[P_{total}]}$. In this equation, $P_{total}$ represent the total amount of protein used. $S_{total}$ represents the total amount of substrate titrated. PS represents the protein/substrate complex. The X-axis is the total substrate concentration used for titration. The y-axis indicates the theoretical percentage of bound fraction. A serial of 0, 4.8, 9.1, 13.0 and 16.7 mM MgATP were titrated into 0.4 mM $SCaMC_{TMD}$ under our NMR titration condition. The corresponding bound fractions as measured from 2D chemical shift for residue D361 were plotted as red dots, which suggest a binding affinity around 1.5 mM.

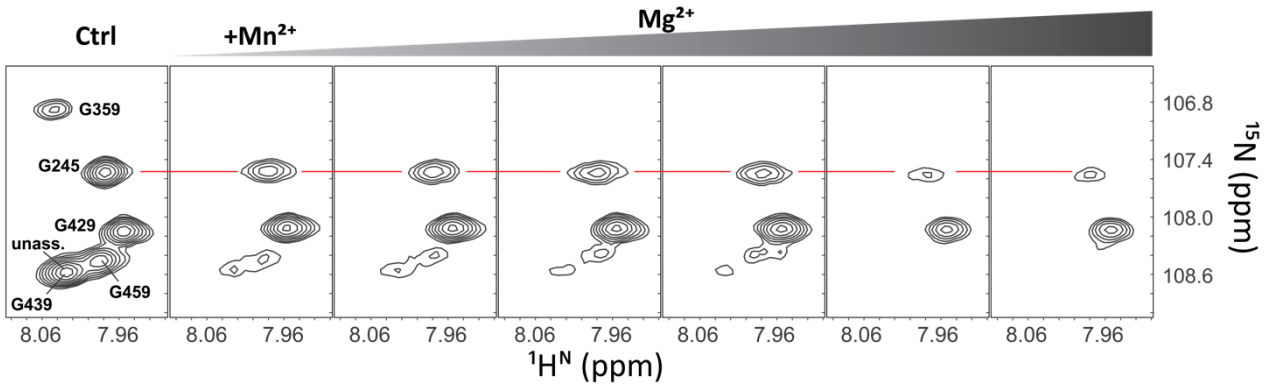


**Figure S4.** The $Mn^{2+}$/$Mg^{2+}$ titration showing the inability of $Mg^{2+}$ cation alone to displace the paramagnetic $Mn^{2+}$. The region from the 2D $^{1}H$-$^{15}N$ TROSY-HSQC spectra, recorded using a 0.5 mM $^{15}N$ labeled sample, is the same as in Fig. 3A&C. The first panel shows peaks in the absence of $Mn^{2+}$ and $Mg^{2+}$. The second panel shows broadening of peaks in the presence of 1.25 mM $Mn^{2+}$. Panels 3 to 7 are spectra recorded at increasing concentrations of $Mg^{2+}$: 5, 10, 15, 20 and 30 mM.

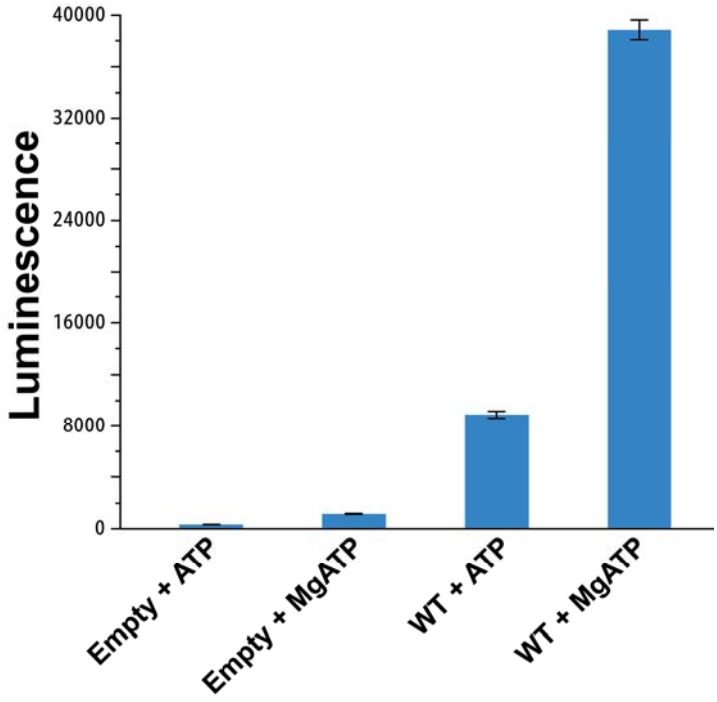


**Figure S5.** The nucleotide transport activity of $SCaMC_{TMD}$ showing a much higher selectivity for MgATP over ATP. The activities were measuring using the proteoliposome assay depicted in Fig. 4A. In the duration of 5 minutes, $SCaMC_{TMD}$ transports about 4.5 times as much MgATP as ATP. Error bars are ± one s.t.d. values determined from 3 repeat measurements.

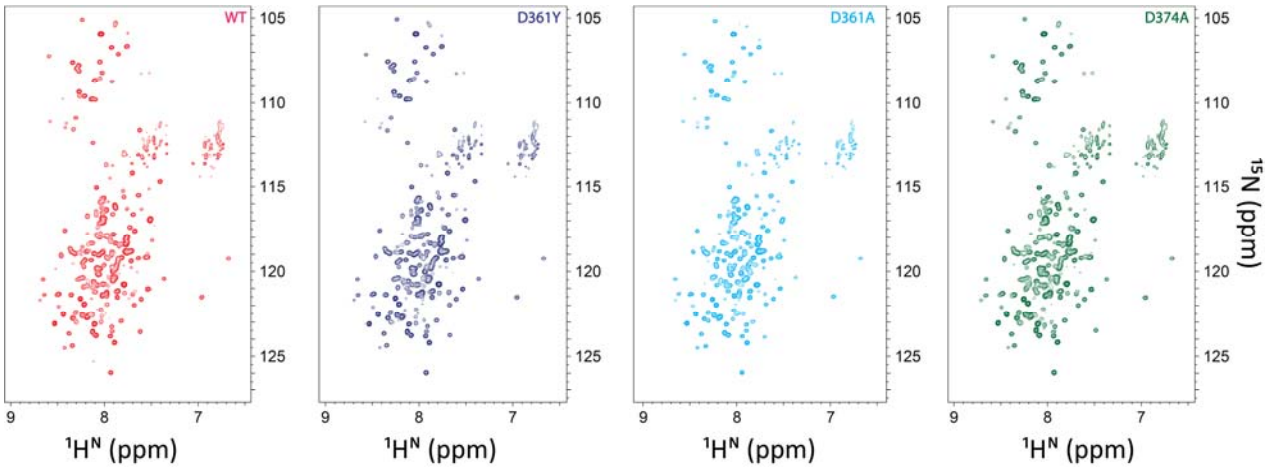


**Figure S6.** Comparison of the NMR spectra of the WT and mutant $SCaMC_{TMD}$ showing negligible effect of the mutations on the overall transporter structure. The 2D $^1H$-$^{15}N$ TROSY-HSQC spectra of the WT, D361Y, D361A and D374A mutants were recorded using 0.5 mM $^{15}N$ labeled protein in the same buffer condition.

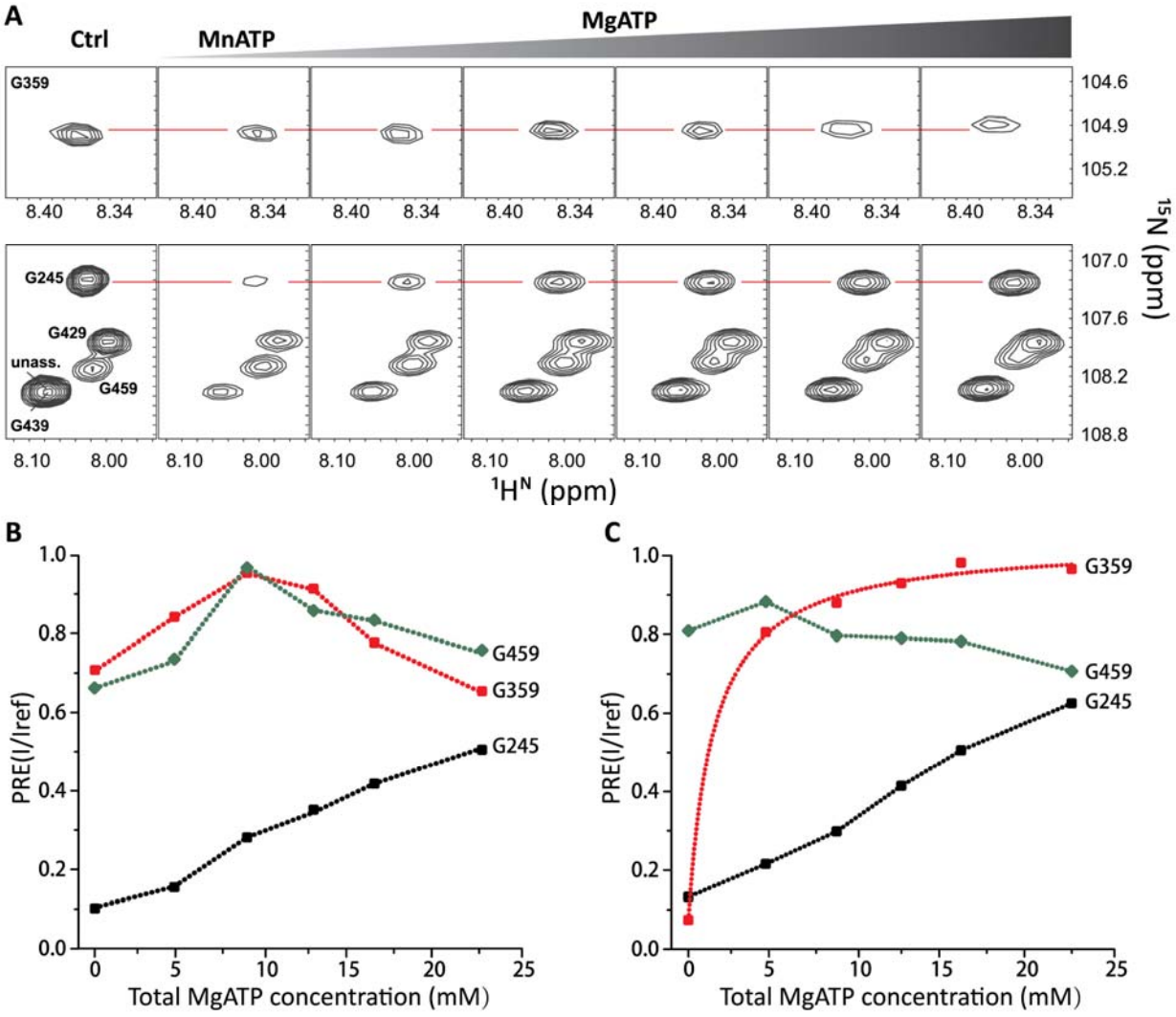


**Figure S7. The D361A mutation abrogates the ability of SCaMC$_{TMD}$ to bind MgATP**

**(A)** The MnATP/MgATP titration showing the inability of MgATP to displace MnATP for the D361A mutant. The region from the 2D $^{1}$H-$^{15}$N TROSY-HSQC spectra, recorded using a 0.5 mM *U*-[$^{15}$N, $^{13}$C, $^{2}$H]-labelled sample, contains the same peaks as in Fig. 3A&C. The first panel shows peaks in the absence of MnATP and MgATP. The second panel shows broadening of peaks in the presence of 1.25 mM MnATP. Panels 3 to 7 are spectra recorded at increasing concentrations of 4.5, 8.69, 12.5, 16.0 and 22.2 mM MgATP.

**(B)** Plots of PRE (normalized peak intensity) vs. MgATP concentration for the D361A mutant for the residues labeled in (A).

**(C)** The same plots as in (B) for the WT SCaMC$_{TMD}$.